Investigation of Transonic Truss-Braced Wing Aircraft Transonic Wing-Strut Interference Effects using FUN3D

Juntao Xiong[1], Jason Fugate[2]
Stinger Ghaffarian Technologies, Inc., Moffett Field, CA 94035

Nhan Nguyen[3]
NASA Ames Research Center, Moffett Field, CA 94035

This paper presents a computational study of transonic wing-strut interference effects of Transonic Truss-Braced Wing (TTBW) aircraft using the high-fidelity CFD code FUN3D. The study is conducted for the wing-strut and the wing-alone configurations at different Mach numbers and Reynolds numbers. The interference effects are calculated by comparing the wing aerodynamics along the spanwise direction between the wing-strut and the wing-alone configurations. The presence of the strut underneath the wing induces a suction peak on the lower surface of the wing, which causes changes in aerodynamic forces and moments, as well as the aerodynamic center location. The interference effects become more pronounced as the Mach number increases. The Reynolds number has less impact on the interference effects. A transonic wing-strut interference aerodynamic correction method is developed for use in a lower-fidelity tool, VSPAERO, coupled to a finite-element model for rapid flutter analysis.

I. Introduction

The demand for green aviation is expected to increase with the need for reduced environmental impact. Most large transports today operate within the best cruise L/D range of 18-20 using the conventional tube-and-wing design. This configuration has led to incremental improvements in aerodynamic efficiency over this past century. In recent years, the use of lightweight materials, such as composites, has been shown to significantly reduce structural weight or trim drag, leading to improve energy efficiency.The Subsonic Ultra Green Aircraft Research (SUGAR) Transonic Truss-Braced Wing (TTBW) aircraft concept is a Boeing-developed N+3 aircraft configuration funded by NASA Aeronautics Research Mission Directorate (ARMD) Advanced Air Transport Technologies (AATT) project.[1-3] The main idea is to use truss structures to alleviate the wing root bending moment, so that a significant increase in the wing aspect ratio could be afforded. Figure 1 is an illustration of the TTBW aircraft. The TTBW aircraft is designed to be aerodynamically efficient by employing an aspect ratio of about 19, which is significantly greater than those of conventional aircraft cantilever wings. As a result, intermediate structural supports are required. The main wings are braced at approximately mid-span by two main struts. In addition, two jury struts, one on each wing, provide additional reinforcement. The additional braced structures will cause some aerodynamic impacts to the wing. The design of a truss-braced wing is a Multidisciplinary Design Optimization (MDO) process that strives to achieve a delicate balance between aerodynamic and structural efficiencies. A typical MDO process uses a variety of different tools of varying fidelity for many different purposes such as aerodynamic prediction, aero-structural analysis,

[1] Aerospace Engineer, Intelligent System Division, juntao.xiong@nasa.gov, AIAA Member
[2] Aerospace Engineer, Intelligent System Division, jason.fugate@nasa.gov
[3] Senior Research Scientist, Intelligent System Division, nhan.t.nguyen@nasa.gov, Associate Fellow AIAA

flutter analysis. CFD is the main tool for aerodynamic prediction. On the other hand, for flight dynamic analysis of stability and control, a lower-order tool may be sufficient during the early stage of the design.

Figure 1. Boeing SUGAR Transonic Truss-Braced Wing (TTBW) Aircraft Concept

A previous study was conducted to investigate the aerodynamic and structural performances of the NASA Generic Transport Model (GTM) aircraft by using a fast low-fidelity potential flow solver VSPAERO coupled with an in-house nonlinear finite-element code BEAM3D. [4-5] The VSPAERO code includes both a low-fidelity vortex-lattice model and a mid-fidelity panel model for steady-state aerodynamics. Transonic and viscous flow corrections for the steady-state aerodynamics are implemented on the vortex-lattice model using a 2D transonic small disturbance (TSD) code called TSFOIL coupled to an in-house integral boundary layer (IBL) code. This suite of tools can rapidly predict the aero-structural performance of the TTBW with good accuracy. Due to the limitation of VSPAERO and the 2D transonic and viscous flow corrections, which cannot capture the 3D transonic and viscous interference effects between the wing and strut, FUN3D, a high-fidelity CFD solver, is used to investigate the impact of the interference in this research. First, a grid independence study of the TTBW aircraft simulation is performed. The computational results are compared with NASA Ames 11-Ft transonic wind tunnel experimental results. Then, the FUN3D solver is used to simulate the wing-strut and wing-alone configurations at different Mach numbers and Reynolds numbers to investigate the transonic interference effects. Based on the simulation results, an interference correction method is developed for the VSPAERO code. The correction improves the predictive capability of VSPAERO for conceptual analysis of the TTBW.

II. Computational Approach

A. Numerical Code

The computational fluid dynamics code used in this study is FUN3D[6-7], which solves the unsteady three-dimensional Navier-Stokes equations on mixed-element grids using a vertices-centered finite-volume method. Information exchange for flow computation on different partitions using multiple CPUs is implemented through the MPI (Message Passing Interface) protocol. It employs an implicit upwind algorithm in which the inviscid fluxes are obtained with a flux-difference-splitting scheme. At interfaces delimiting neighboring control volumes, the inviscid fluxes are computed using an approximate Riemann solver based on the values on either side of the interface. The Roe's flux difference splitting[8] is used in the current study. For second-order accuracy, interface values are obtained by extrapolation of the control volume centroidal values, based on gradients computed at the mesh vertices, using an unweighted least-squares technique. The Venkatakrishnan[9] limiter is used in the current study to limit the reconstructed values when necessary. In this study the tetrahedral with prism meshes are used. In FUN3D, for tetrahedral

meshes, the full viscous fluxes are discretized using a finite-volume formulation in which the required velocity gradients on the dual faces are computed using the Green-Gauss theorem. The solution at each time-step is updated with a backwards Euler time-differencing scheme. At each time step, the linear system of equations is approximately solved with either a multi-color point-implicit procedure or an implicit-line relaxation scheme. Local time-step scaling is employed to accelerate convergence to steady-state. To model turbulent flows, the one-equation model of Spalart-Allmaras[10] (S-A) is used in this study.

B. Computational Model and Grid

In this paper, two Mach 0.745 TTBW Outer Mold Line geometries are studied: cruise 1g shape geometry and jig shape geometry. The geometries for the Mach 0.745 TTBW are based on the CAD models of the 765-095-200_RJ version. The jig shape geometry is not a flight jig shape which accounts for the wing aeroelastic wash-out twist for the full-scale vehicle at the design flight condition, but is a wind tunnel model jig shape. Wind tunnel tests of the 1g shape geometry have been conducted in NASA Ames 11-Ft Transonic Wind Tunnel. First, two configurations of the TTBW 1g shape geometry are used for the grid independence study and simulation validation. Figure 2 illustrates the TTBW 1g shape geometry config-24, which includes all the aircraft components. Figure 3 shows the surface mesh of the geometry. The volume mesh is comprised of tetrahedral elements and a prism layer near the wall. The prism layer is used to resolve the turbulent boundary layer. In the grid-independence study, two different mesh sizes: medium and fine, with a total of 62 million and 90 million nodes, respectively, are used.

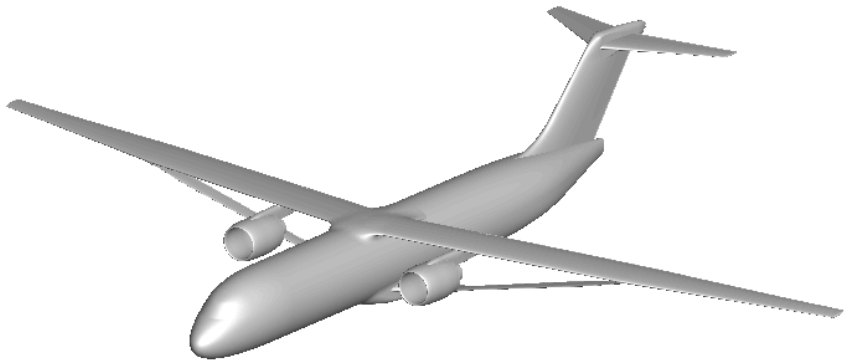

Fig. 2 TTBW 1g Shape Geometry config-24

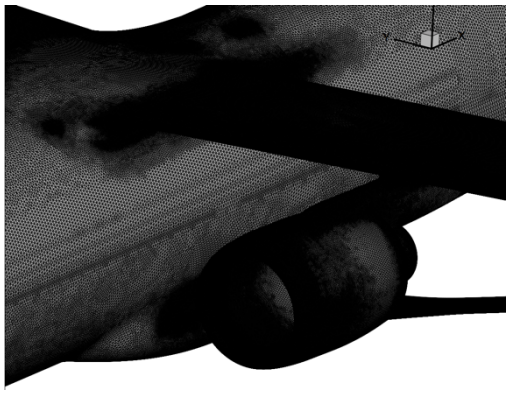

Fig. 3 Computational Grid

After validation, the wing-strut interference effects are studied. In this paper, in order to save the computation expenses the engine and the horizontal tail are not modelled since we only focus on studying the wing-strut interference effects. Figure 4 shows the configurations of the TTBW geometry which are used to investigate the interference effects.

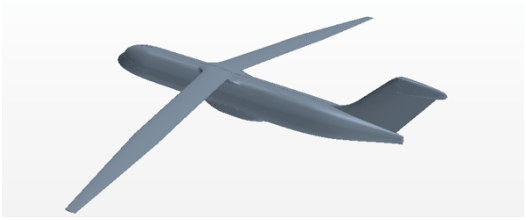

(a) Wing-alone Configuration

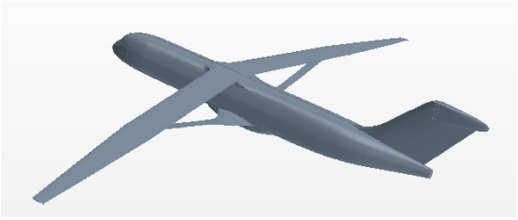

(b) Wing-strut Configuration

Fig. 4 TTBW Configurations

III. Results

The grid independence study is performed for the TTBW 1g shape geometry config-24, and the computation results are validated with experimental data for the TTBW 1g shape geometry config-24 and config-21. The config-21 geometry does not include the engine/pylon and horizontal tail. Wind tunnel test data of the 1g shape geometry in NASA Ames11-Ft Transonic Wind Tunnel are available for validation. Test data from Run 363 at Mach 0.745 and Reynolds number of 3.3 million based on the mean aerodynamic chord (MAC) with full wind tunnel model corrections are used for the config-24 validation. Test data from Run 290 at Mach 0.745 and Reynolds number of 3.3 million based on the MAC with full wind tunnel model corrections are used for the config-21 validation. After the validation, FUN3D code is used to simulate the Wing-strut and wing-alone configurations which are shown in Fig. 4 and to determine the interference effects at different Mach numbers and Reynolds numbers. Based on the simulation results, an interference correction method is developed for the VSPAERO code.

A. Grid-independence Study and Validation

The presentation of the results begins with a comparison between aerodynamic forces obtained both experimentally via wind tunnel testing, and computationally via FUN3D at different levels of mesh refinement for the TTBW 1g shape geometry config-24 for Mach 0.745 and a Reynolds number of 3.3 million. Figure 5 shows the lift and drag coefficients computed by FUN3D on the two different meshes as well as wind tunnel Run 363 data. The differences of the predictions on the two different meshes are small. The simulated lift coefficients between different mesh sizes are almost identical. The differences of the simulated drag coefficients by using the two meshes are less than 10 counts all through the drag polar. Therefore, grid independence has been achieved. Compared to the experimental data, FUN3D slightly over predicts the lift coefficient. There is an angle of attack shift of approximately 0.3 degrees between the two lift curves. The drag polar computed by FUN3D shows very good agreement with the wind tunnel data. The difference in the drag coefficient at the same lift coefficient is less than 5 counts. Figure 6 shows the surface pressure coefficient distribution at one simulated flight condition of config-24. There is a weak shock structure on the wing, which helps to improve the lift coefficient with a small drag penalty at transonic conditions. To further validate the FUN3D simulation results, another set of wind tunnel data Run 290 for config-21 is used. Figure 7 shows the lift and drag coefficients computed by FUN3D as well as wind tunnel Run 290 data of the TTBW 1g shape geometry config-21 for Mach 0.745 and a Reynolds number of 3.3 million. Similar to the config-24 comparison, FUN3D also over predicts the lift coefficient for config-21.

There is an angle of attack shift of about 0.4 degrees in this case. The drag polar computed by FUN3D shows an excellent agreement with the wind tunnel data. The two drag polar curves almost are almost identical. Figure 8 shows the surface pressure coefficient distribution at one simulated flight condition of config-21. The close agreements with wind tunnel data provide confidence in the FUN3D prediction for further investigating the transonic wing-strut interference effects.

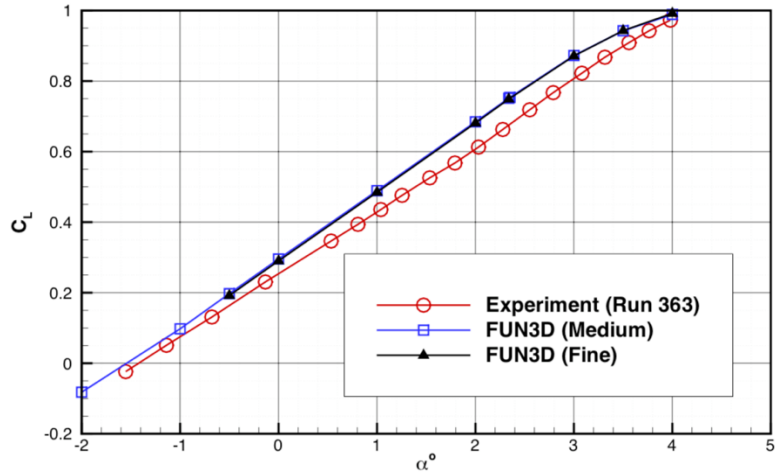

(a) Lift Curve

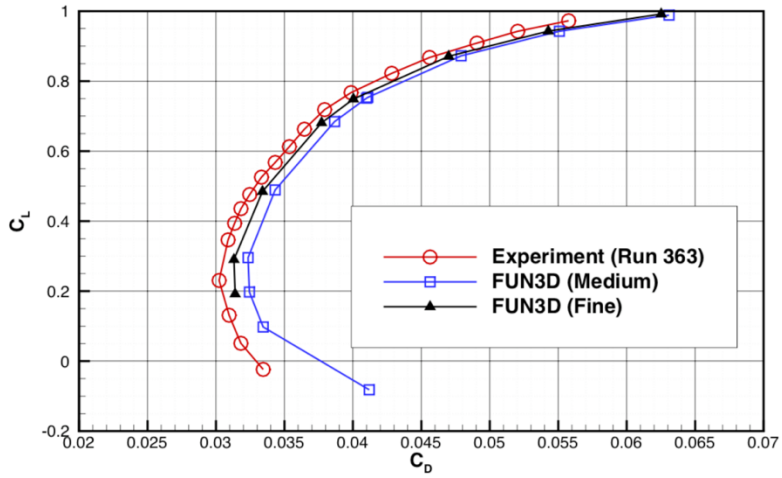

(b) Drag Polar

Fig. 5 Comparison of Lift and Drag Predictions for the TTBW 1g Shape Geometry Config-24 (Ma = 0.745, Re = 3.3×10^6)

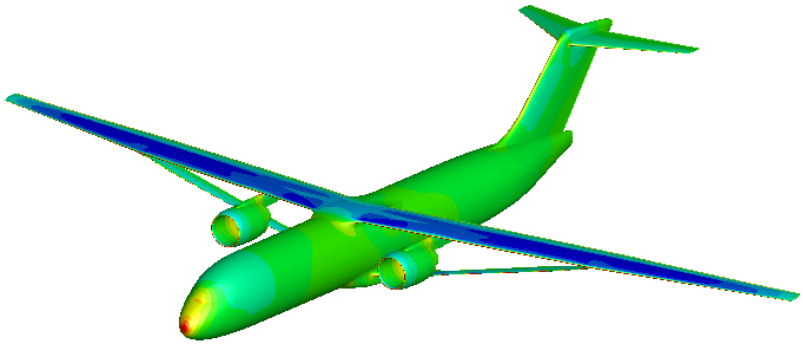

Fig. 6 Pressure Coefficient Contour on the TTBW 1g Shape Geometry Config-24 Surface (Ma = 0.745, C_L= 0.73, Re = 3.3×10^6)

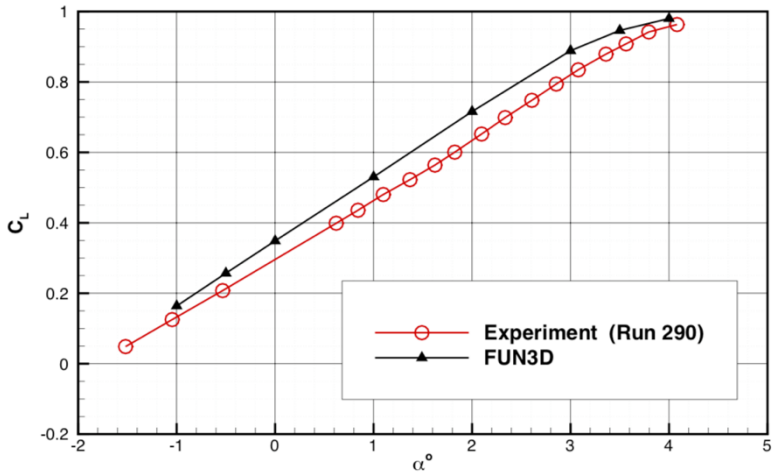

(a) Lift Curve

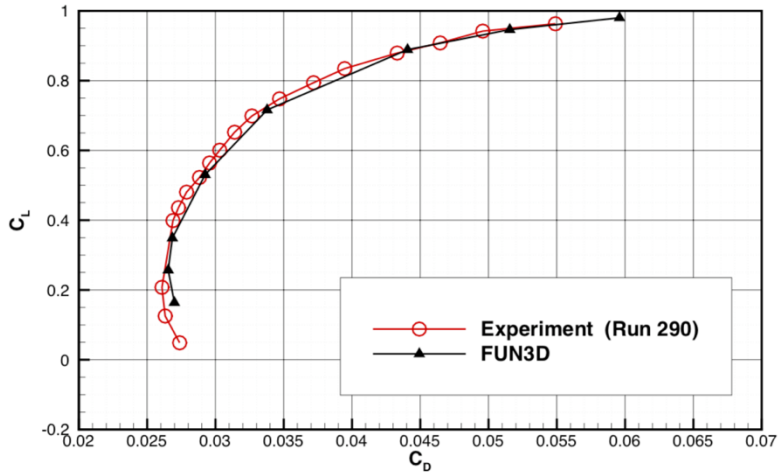

(b) Drag Polar

Fig. 7 Comparison of Lift and Drag Predictions for the TTBW 1g Shape Geometry Config-21 (Ma = 0.745, Re = 3.3×10^6)

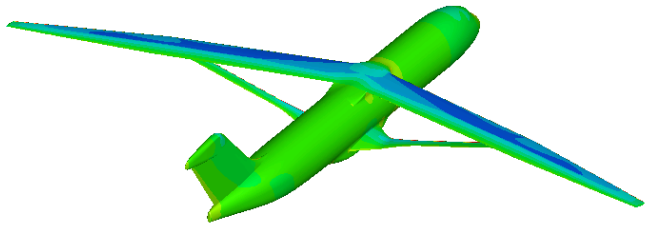

Fig. 8 Pressure Coefficient Contour on the TTBW 1g Shape Geometry Config-21 Surface (Ma = 0.745, C_L= 0.73, Re = 3.3×10^6)

B. Reynolds number effect of the wing-strut interference

The wing-strut interference effects are investigated by determining the difference in the wing sectional aerodynamic coefficients between the wing-alone and the wing-strut configurations which are shown in Fig. 4.

The Reynolds number effect on the wing-strut interference is first investigated. Figures 9-10 show the pressure coefficient distributions at five wing span locations at zero angle of attack for Mach number 0.745 and two Reynolds numbers, 3.3 million and 11.9 million. The pressure distributions for the wing-alone configuration are not shown in the figures. At high Reynolds number (Re=11.9 million), although the shock wave is slightly intensified relative to the low Reynolds number (Re=3.3 million) case, there is no significant change in the overall interference effect. The pressure differences are small at the in-board of the wing where the distance between the wing and strut is large. Near the wing-strut juncture location, a suction peak appears on the lower surface of the wing. The pressure difference decreases toward the out-board of the wing where the interference effects are diminished.

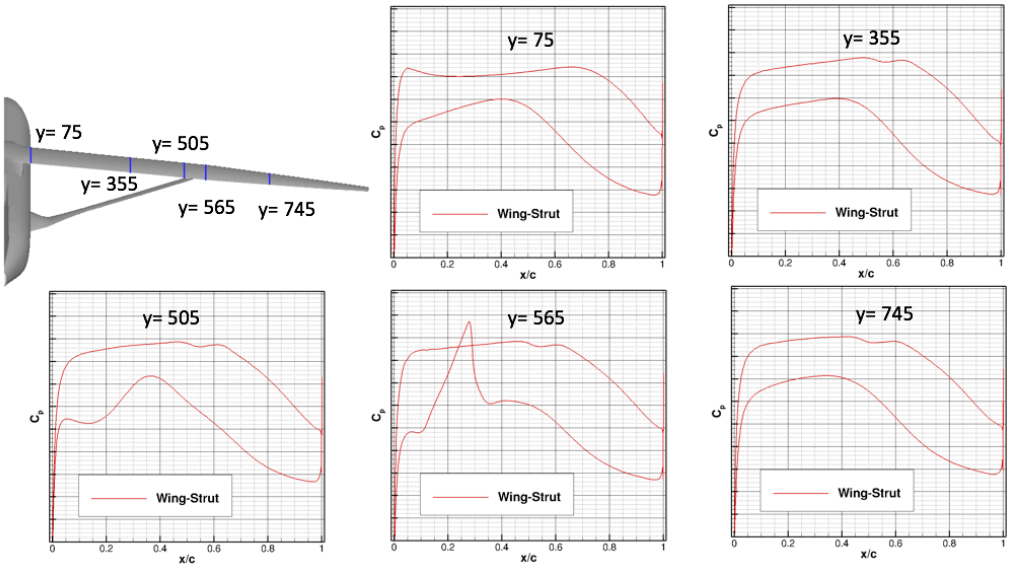

Fig. 9 Comparison of Pressure Coefficient (Ma = 0.745, α = 0.0°, Re = 3.3×10^6)

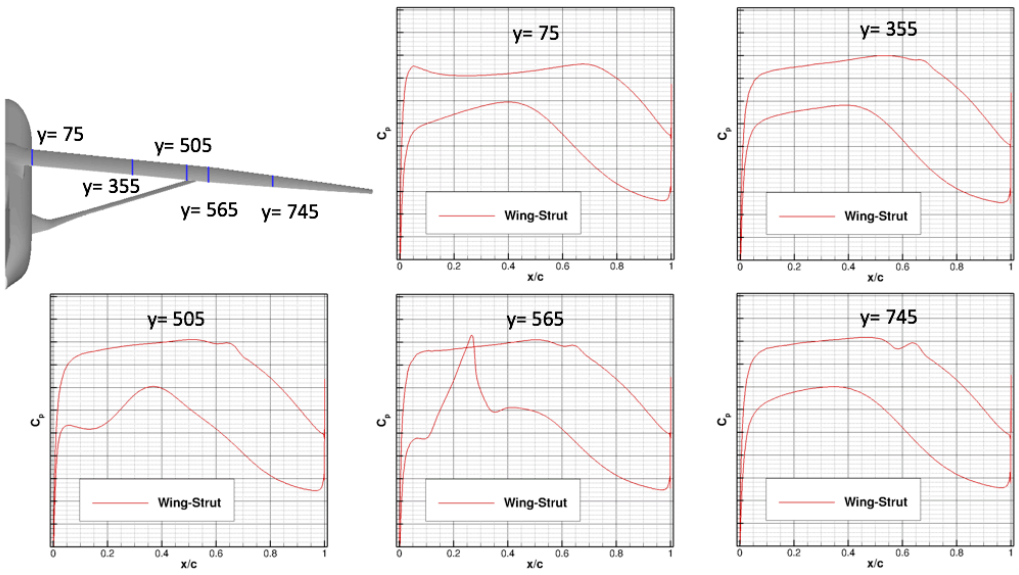

Fig. 10 Comparison of Pressure Coefficient (Ma = 0.745, α = 0.0°, Re = 11.9×10⁶)

C. Mach number effect of the wing-strut interference

In order to investigate the Mach number impact on the wing-strut interference, four different Mach numbers 0.3, 0.745, 0.8, and 0.85 are simulated. Figure 11 (a)-(e) shows the pressure coefficient distributions at five wing span locations for the four Mach numbers and Reynolds number 3.3 million, and an angle of attack of 2 degrees. The pressure distributions for the wing-alone configuration are not shown in the figures. At the low Mach number 0.3, the interference effects are found to be negligible. The pressure coefficient distributions at the five wing span locations are very similar for low Mach number.

At the Mach number 0.745, there are relatively small differences in the pressure coefficient distributions on the wing surface at the wing in-board station. The shock wave is slightly stronger on the upper surface of the wing for the wing-strut configuration which causes the lift coefficient to increase at the wing in-board 75 station. Near the wing-strut juncture 565 station a small suction peak appears on the lower surface of the wing. At the wing out-board 745 station, the pressure coefficient distributions are almost the same.

As the Mach number increases to 0.80 and 0.85, the difference in the pressure coefficient distributions are seen to become increasingly significant and are most pronounced on the lower surface of the wing near the juncture location. A high-speed flow region on the lower surface is indicated by the sharp decrease in the surface pressure coefficient. At high Mach number the presence of the wing-strut juncture apparently changes the entire pressure distribution along the wing and makes the shock wave stronger, especially at Mach number 0.85, which will cause a strong shock on the wing surface which in turn deteriorates the aerodynamic performance.

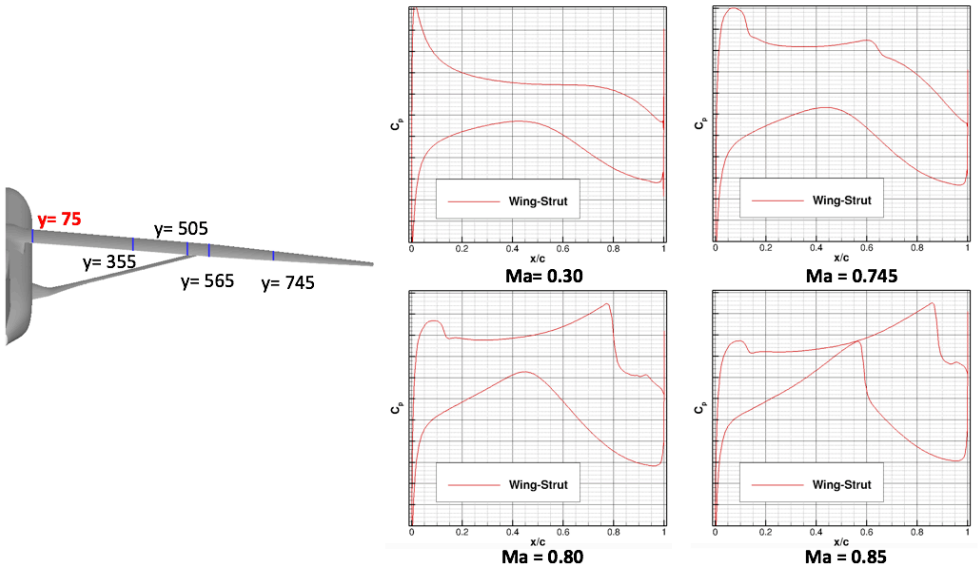

(a) y = 75 inch

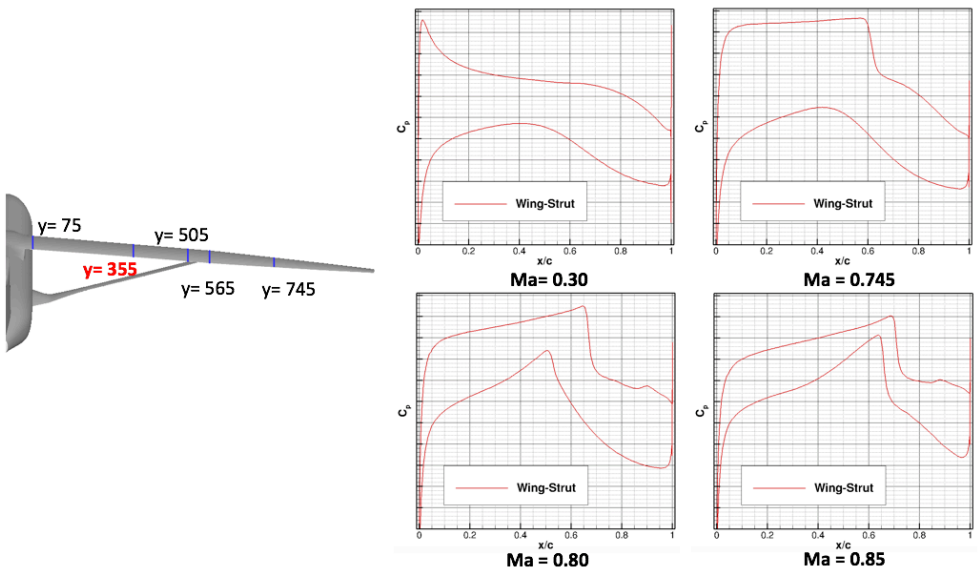

(b) y = 355 inch

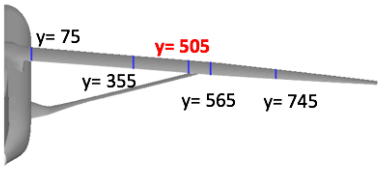

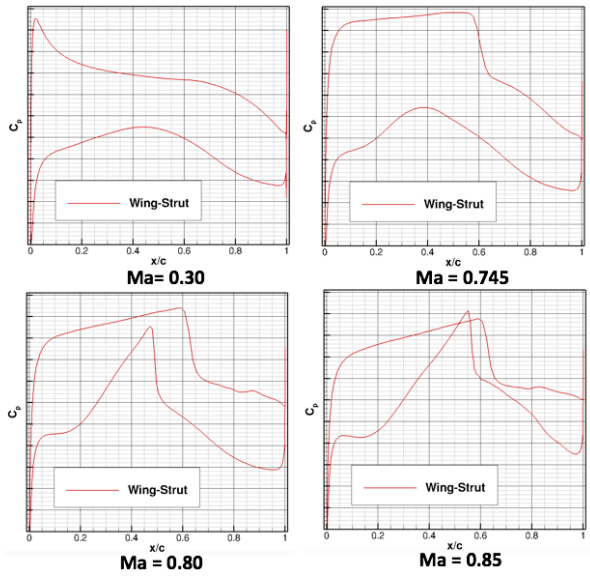

(c) y = 505 inch

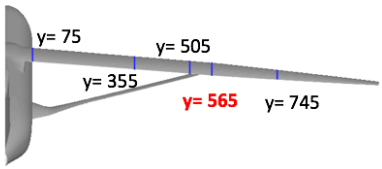

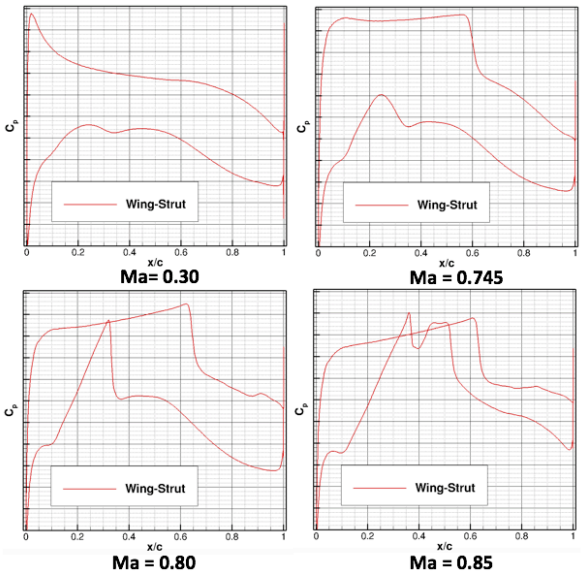

(d) y = 565 inch

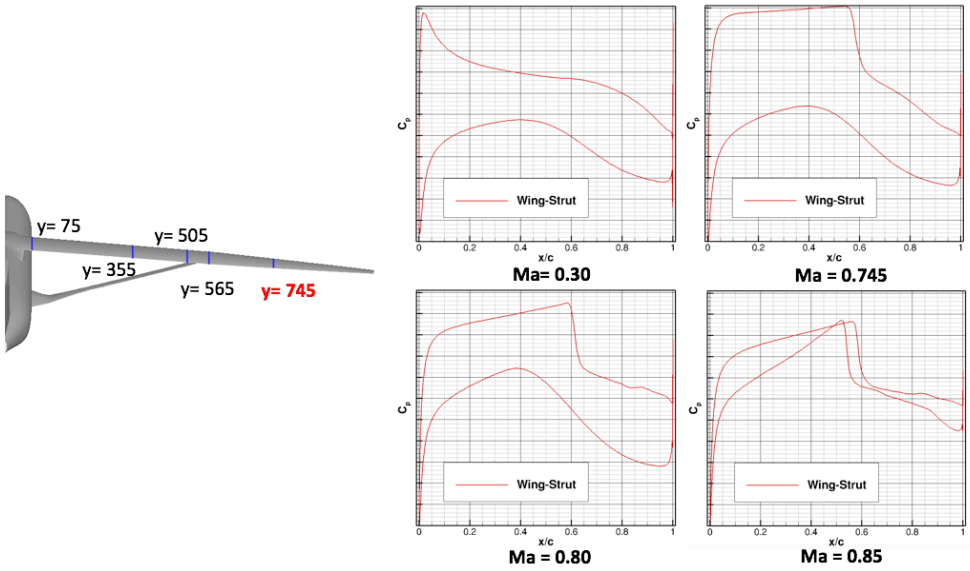

(e) y = 745 inch

Fig. 11 Comparison of Pressure Coefficient (α = 2.0°, Re = 3.3✕10⁶)

D. Interference correction implementation

In this section a transonic wing-strut interference correction method is developed to correct the VSPAERO model coupled to the TSD/IBL method using the FUN3D simulation data. VSPAERO is a potential flow solver which has been implemented with a 2D transonic and viscous flow corrections via the TSD/IBL method. More details about VSPAERO coupled with the TSD/IBL method can be found in Ref. 3.

The wing-strut interference effects are calculated by determining the difference in the wing sectional aerodynamic coefficients between the wing-alone and the wing-strut configurations as shown in Fig. 4. The correction terms are calculated by using Eq. 1.

$$\Delta c_{IC} = \underbrace{\left(dc_{FUN3D}}_{\text{3D Transonic / Viscous Interference}} - \underbrace{dc_{VSPAero+TSD/IBL}\right)}_{\text{3D Inviscid Interference + 2D Transonic / Viscous Corrections}} \tag{1}$$

Where c represents a key aerodynamic parameter such as c_L , c_D, c_M, and c_{L_α}. dc represents the change in the given parameter between geometric configurations such as wing-strut and wing-alone configurations. Figure 12 shows the lift distribution and the sectional lift coefficient correction along the wing span for Mach number 0.745, C_L = 0.4536, Reynolds number 3.3 million. The presence of the strut enhances the shock wave at the upper surface of the wing at in-board wing stations which increases the lift coefficient. There is an abrupt change in the lift coefficient near the wing-strut juncture location which is caused by the suction peak on the lower surface of the wing. The lift coefficient difference decreases toward the out-board of the wing where the interference effects are diminished. For the implementation of the wing-strut interference correction piecewise polynomials are used to fit the data for the in-board wing stations. Near the strut and the out-board wing stations, two discontinuous linear fits are used where the discontinuity occurs at the wing-strut juncture location.

Figure 13 shows the drag distribution and the sectional drag coefficient correction along the wing span for Mach number 0.745, C_L = 0.4536, Reynolds number 3.3 million. There is an abrupt change in the drag coefficient near the wing-strut juncture location for FUN3D simulation results which is caused by the suction peak on the lower surface of the wing. The VSPAERO+TSD/IBL could not capture the change of the sectional drag coefficient near the wing-strut juncture location due to its limitation, which need to be corrected. The piece-wise polynomials are used to fit the drag coefficient correction distribution for the in-board wing stations and near the strut, and a linear fit is used for the out-board wing stations.

Figure 14 shows the pitching moment distribution and the sectional pitching moment coefficient correction along the wing span direction for Mach number 0.745, C_L = 0.4536, Reynolds number 3.3 million. The pitching moment is calculated about the quarter chord location. The presence of the wing-strut juncture only changes the pitching moment coefficient near the juncture location because the suction peak on the lower surface of the wing reshapes the pressure distribution on the wing. A piecewise polynomial is used to fit the sectional pitching moment coefficient correction near the strut, and two linear fits are used for the in-board and out-board wing stations.

It should be noted that for the correction procedure, piecewise polynomials are used to fit the correction data. A scale is established for each segment so that the corresponding interference correction can be calculated at any given span station based on the aircraft lift coefficient. Certain regions along the span, which are fit by the linear curves depicted in red, are found to have no direct correlation to the lift coefficient. Thus, the interference effect in these regions is treated as constant with varying aircraft lift coefficient. It should also be noted that these curve fitting techniques allow for scalability based on aircraft lift; however, changes to the Mach number would necessitate the establishment of new scales. The impact of varying Reynolds number on aerodynamic interference is found to be marginal via FUN3D; therefore, the established relationships are deemed sufficient for all Reynolds numbers investigated.

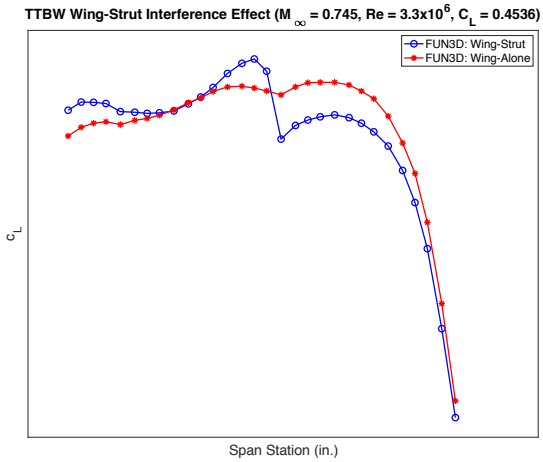

(a) Lift Coefficient Distribution - FUN3D

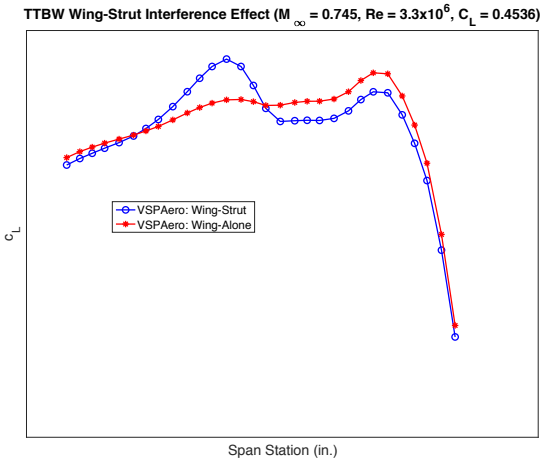

(b) Lift Coefficient Distribution - VSPAERO

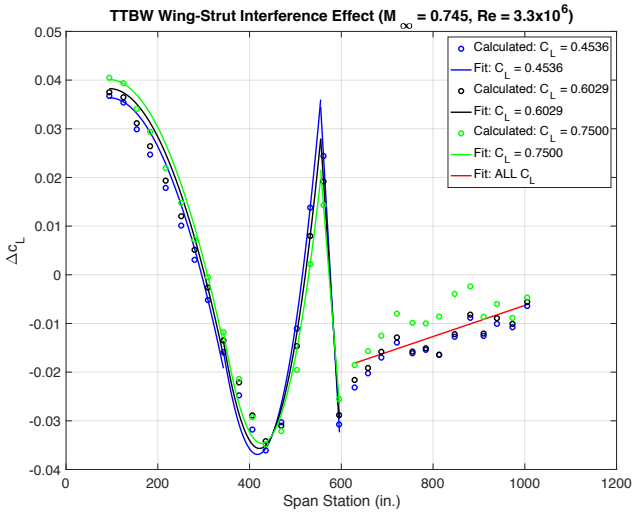

(c) Lift Coefficient Correction Distribution

Fig. 12 Lift Coefficient and Lift Coefficient Correction Distribution (Ma = 0.745, Re = 3.3×10^6)

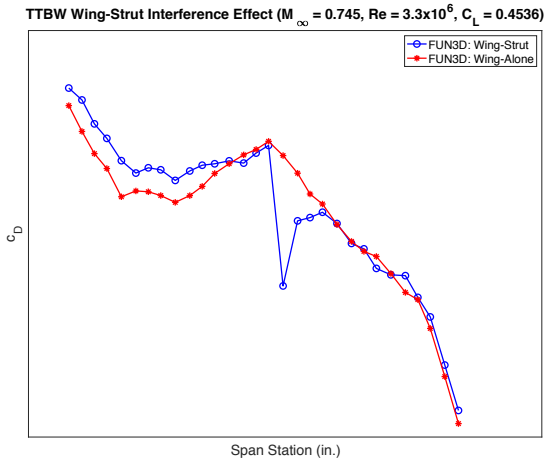

(a) Drag Coefficient Distribution - FUN3D

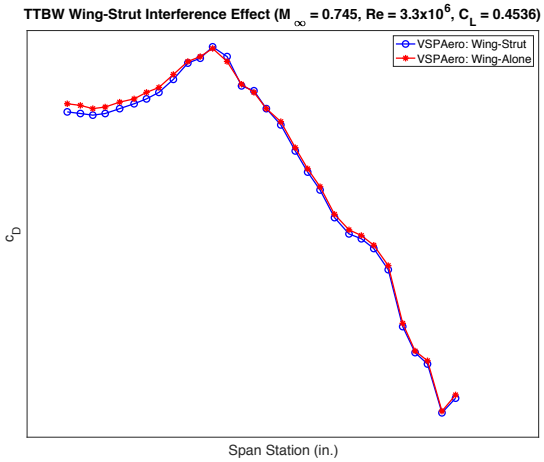

(b) Drag Coefficient Distribution - VSPAERO

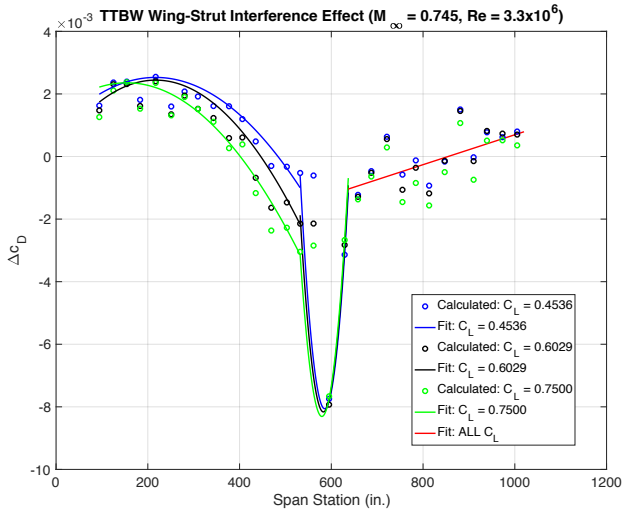

(c) Drag Coefficient Correction Distribution

Fig. 13 Drag Coefficient and Drag Coefficient Correction Distribution (Ma = 0.745, Re = 3.3×10^6)

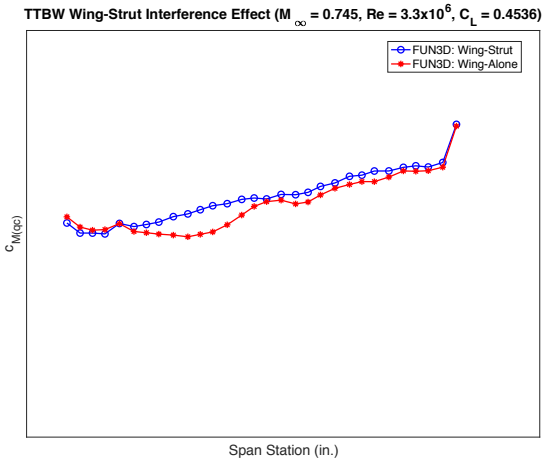

(a) Moment Coefficient Distribution – FUN3D

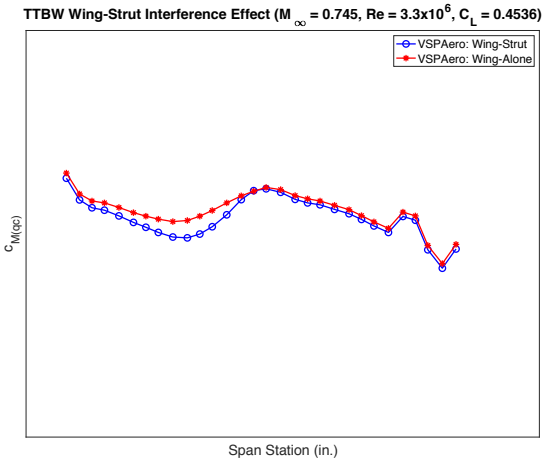

(b) Moment Coefficient Distribution – VSPAERO

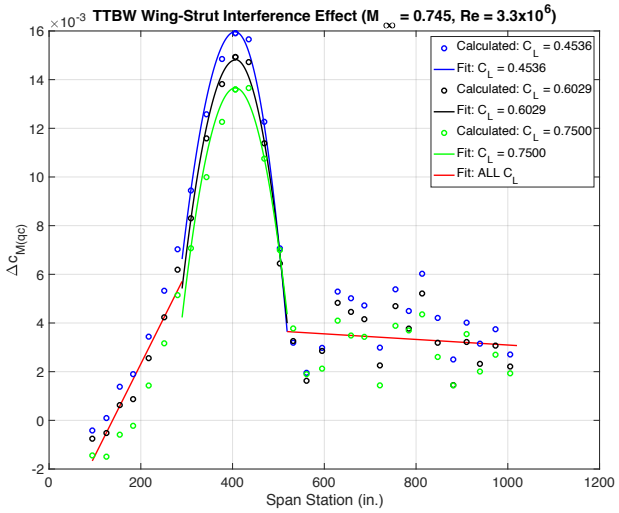

(c) Moment Coefficient Correction Distribution

Fig. 14 Moment Coefficient and Moment Coefficient Correction Distribution (Ma = 0.745, Re = 3.3✕10⁶)

The interference effects on two other key aerodynamic parameters, namely the sectional c_{L_α} and sectional aerodynamic center location x_{ac} are also investigated. Figure 15 shows sectional c_{L_α} and the correction for wing-strut interference, whereas Fig.16 shows the aerodynamic center and the correction for wing-strut interference. For the case of c_{L_α}, it can be seen that a sharp drop in the correction occurs near the wing-strut juncture, while the remaining wing span stations experience a relatively smaller correction. The aerodynamic center location is found to be shifted very slightly forward near the juncture and slightly backward inboard of the juncture where the presence of the strut still has a noticeable impact on the aerodynamic center location. A numerically complex piecewise spline could be used to fit the c_{L_α} and x_{ac} interference correction data along the wing span. The applied correction for the x_{ac} could be assumed as constant for the various flight conditions being simulated as long as Mach number is maintained.

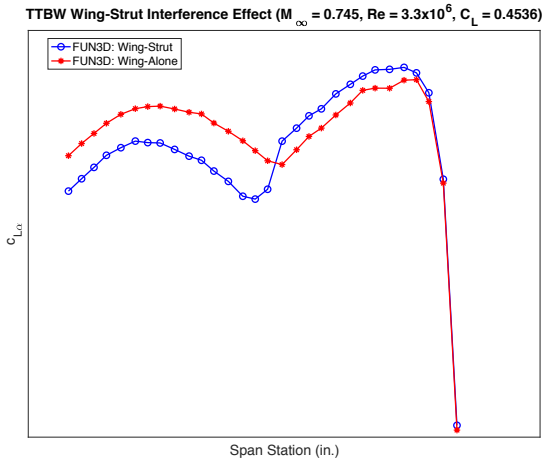

(a) Lift Curve Slope - FUN3D

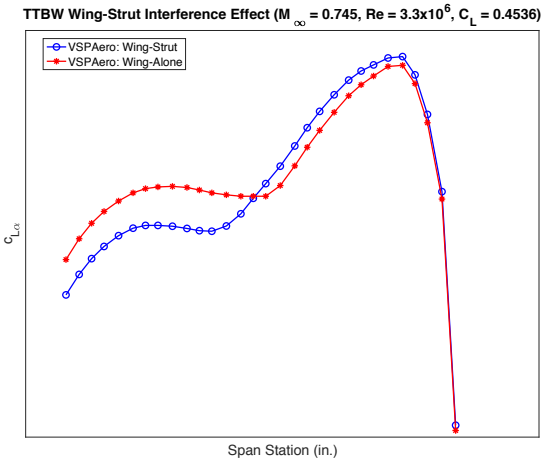

(b) Lift Curve Slope - VSPAERO

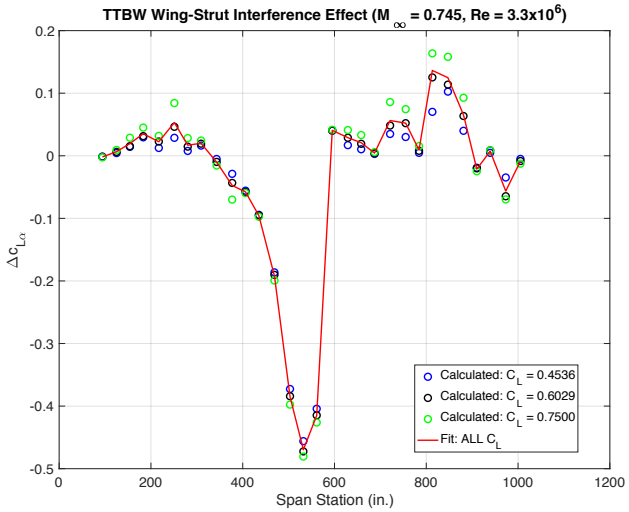

(c) Lift curve slope correction distribution

Fig. 15 Lift curve slope and Lift curve slope Correction Distribution (Ma = 0.745, Re = 3.3×10⁶)

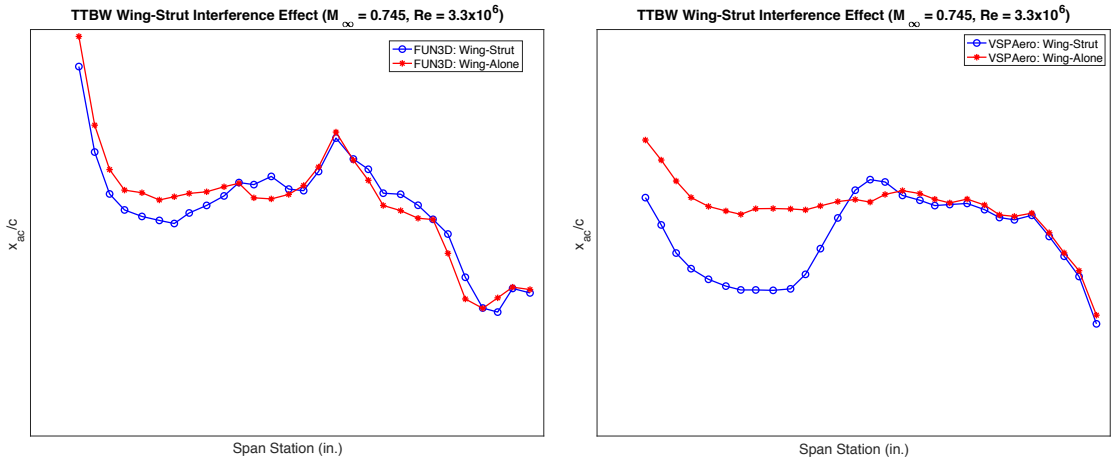

(a) Aerodynamic Center Distribution - FUN3D (b) Aerodynamic Center Distribution -VSPAERO

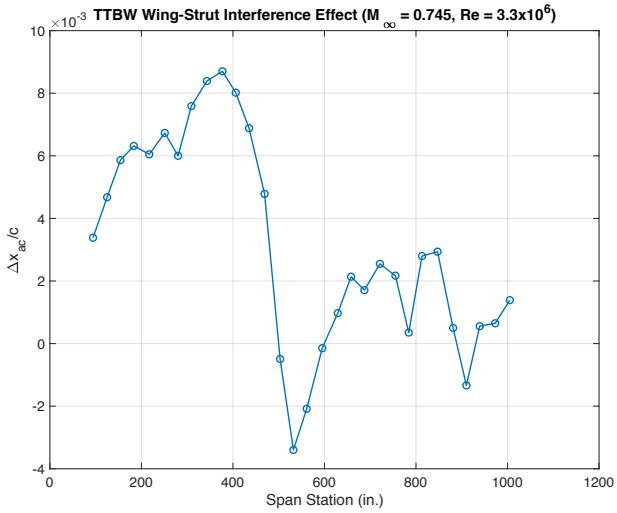

(c) Aerodynamic Center correction distribution

Fig. 16 Aerodynamic Center and Aerodynamic Center Correction Distribution (Ma = 0.745, Re = 3.3×10^6)

The correction method is applied to the VSPAERO+TSD/IBL model to update the sectional lift, drag, and pitching moment coefficients of each wing section. As can be seen, near the strut juncture region, there is a significant change in aerodynamic performance. The wing-strut interference correction is generally small at Mach 0.745, but can become larger as the Mach number increases. With the interference correction terms applied, the VSPAERO+TSD/IBL model is used for the aerodynamic analysis of the cruise 1g shape TTBW geometry and for the aero-structural analysis of the jig shape TTBW geometry.[3,11] Figure 17 shows the lift and drag coefficients computed by VSPAERO for Mach 0.745 and a Reynolds number of 3.3 million with and without all the corrections. These computed results are compared to wind tunnel Run 363 data. While the lift coefficient is somewhat under-predicted, the drag coefficient computed by VSPAERO alone is mostly due to induced drag and therefore is substantially under-predicted. With all the corrections applied to the VSPAERO model for transonic viscous flow and wing-strut interference aerodynamics, the lift and

drag coefficients match remarkably well with the wind tunnel data, although there is a small discrepancy in the drag polar at lower lift coefficients. The excellent agreement between the VSPAERO+TSD/IBL model and the wind tunnel Run 363 data thus validates the aerodynamic modeling approach. The VSPAERO TSD/IBL with the wing-strut interference correction model can be used as a rapid and reliable tool for the TTBW aircraft conceptual analysis and design.

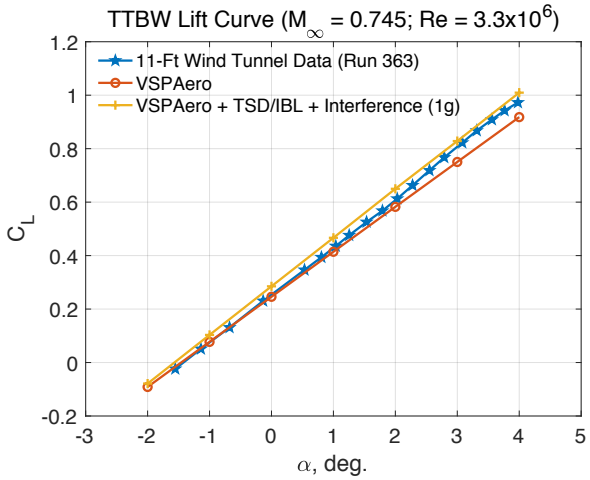

(a) Lift curve

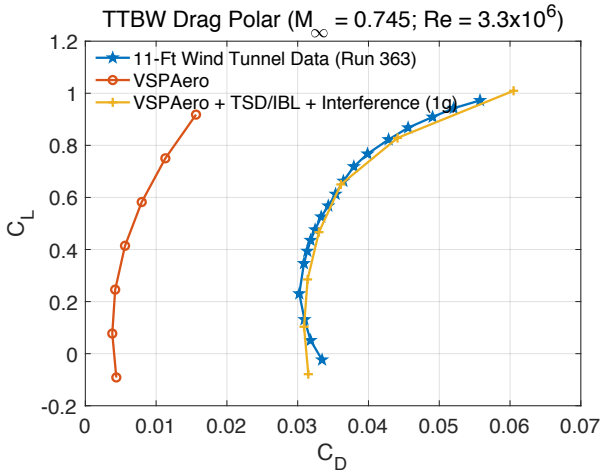

(b) Drag Polar

Fig. 17 Lift Curve and Drag Polar (Ma = 0.745, Re = 3.3×10^6)

IV. Conclusions

A computational investigation of the wing-strut interference effect for the TTBW aircraft is presented. The presence of the strut underneath the wing induces a suction peak on the lower surface of the wing, which causes an abrupt change in the aerodynamic forces, pitching moments, and aerodynamic center location. The interference effects increase as the Mach number increases. There is less impact of the Reynolds number effect on the interference. With the developed interference correction method in conjunction with the transonic viscous flow corrections via the TSD/IBL method, the VSPAERO model can be used as a reliable tool for the TTBW aircraft analysis and design.

V. Acknowledgment

The authors wish to acknowledge NASA Advanced Air Transport Technologies project for the funding support of this work.

References

1. Bradley, M. K. and Droney, C. K., "Subsonic Ultra Green Aircraft Research: Phase I Final Report," NASA Contractor Report NASA/CR-2011-216847, Boeing Research and Technology, April 2011
2. Bradley, M. K., Droney, C. K., and Allen, T. J., "Subsonic Ultra Green Aircraft Research Phase II: N+4 Advanced Concept Development," NASA Contractor Report NASA/CR-2012-217556, Boeing Research and Technology, May 2012
3. Nguyen, N., Fugate, J., Xiong, J. and Kaul, U., "Flutter Analysis of the Transonic Truss-Braced Wing Aircraft Using Transonic Correction", AIAA SciTech conference, AIAA-2019-0217, San Diego, CA, Jan. 2019
4. Nguyen, N., Ting, E., and Lebofsky, S. "Aeroelasticity of Axially Loaded Aerodynamic Structures for Truss-Braced Wing Aircraft", AIAA SciTech conference, AIAA-2015-1840, Kissimmee, Florida, Jan. 2015
5. Ting, E., Nguyen, N. and Trinh, Khanh "Static Aeroelastic and Longitudinal Trim Model of Flexible Wing Aircraft Using Finite-Element Vortex-Lattice Coupled Solution", AIAA SciTech conference, AIAA-2014-0837, National Harbor, Maryland, Jan. 2014
6. Biedron, R. T., et al. "FUN3D Manual 13.2", NASA TM-2017-219661, Aug. 2017
7. Lee-Rausch, E. M., Hammond, D. P., Nielsen, E. J., Pirzadeh, S. Z., and Rumsey, C. L., "Application of the FUN3D Unstructured-Grid Navier-Stokes Solver to the 4th AIAA Drag Prediction Workshop cases," AIAA Paper 2010-4511, June. 2010.
8. Roe, P. L., "Approximate Riemann Solvers, Parameter Vectors and Difference Schemes," *Journal of Computational Physics,* Vol. 46, No. 2, 1980, pp. 357–378
9. Venkatakrishnan, V., "Convergence to Steady State Solutions of the Euler Equations on Unstructured Grids with Limiters," Journal of Computational Physics, Vol. 118, No. 1, 1995, pp. 120–130
10. Spalart, P. R. and Allmaras, S. R., "A One-Equation Turbulence Model for Aerodynamic Flows," AIAA 1992-0439, Jan. 1992.
11. Fugate, J., Nguyen, N. and Xiong, J. "Aero-Structural Modeling of the Truss-BracedWing Aircraft Using Potential Method with Correction Methods for Transonic Viscous Flow andWing-Strut Interference Aerodynamics", AIAA Aviation conference, Dallas, TX, June. 2019